DRAFT VERSION NOVEMBER 6, 2018
Preprint typeset using LaTeX style emulateapj v. 5/2/11

WHAT DRIVES THE M_*–SFR RELATION TURNING OVER AT HIGH MASSES? THE ROLE OF BULGES

ZHIZHENG PAN[1], XIANZHONG ZHENG [4], WEIPENG LIN [1,5], JINRONG LI[2,3], JING WANG[6], LULU FAN[7], XU KONG[2,3]

Draft version November 6, 2018

ABSTRACT

It is unclear whether bulge growth is responsible for the flattening of the star formation main sequence (MS) at the high mass end. To investigate the role of bulges in shaping the MS, we compare the NUV–r color between the central ($r < R_{50}$) and outer regions for a sample of 6401 local star-forming galaxies. The NUV–r color is a good specific star formation rate indicator. We find that at $M_* < 10^{10.2} M_\odot$, the central NUV–r is on average only ~ 0.25 mag redder than the outer NUV–r. Above $M_* = 10^{10.2} M_\odot$, the central NUV–r becomes systematically much redder than the outer NUV–r for more massive galaxies, indicating that the central bulge is more evolved at the massive end. When dividing the galaxies according to their Sérsic index n, we find that galaxies with n>2.0 tend to be redder in the central NUV–r color than those with n<2.0, even at fixed B/T and M_*. This suggests that star formation in bulges is more strongly dependent on n (or central mass density) than on B/T. Finally, we find that the fraction of galaxies with n>2.0 rapidly increases with M_* at $M_* > 10^{10.2} M_\odot$, which is consistent with the turning over of the MS at the same transition mass. We conclude that the increasing fraction of low-sSFR dense bulges in $M_* > 10^{10.2} M_\odot$ galaxies, rather than increasing B/T, is responsible for the flattened slope of the M_*–SFR relation at high masses.

Subject headings: galaxies: evolution – galaxies: star formation

1. INTRODUCTION

For star-forming galaxies (SFGs), a tight correlation is found between stellar mass (M_*) and star formation rate (SFR), which is commonly referred to the star formation main sequence (MS) (Brinchmann et al. 2004; Daddi et al. 2007; Elbaz et al. 2007; Guo et al. 2013). The MS can be described by a single pow-law formulated by $\log SFR \propto \alpha \log M_* + \beta$, where α is between 0.6 and 1.0 (Peng et al. 2010; Karim et al. 2011; Whitaker et al. 2012). Recently, the form of the MS is found to be better fitted by two power-laws. Below a transition mass of $M_* \sim 10^{10.2} M_\odot$, the MS has a steep slope of $\alpha \sim 1.0$. Above the transition mass, the slope becomes flattened, with $\alpha = [0.2, 0.8]$, depending on redshift z (Whitaker et al. 2014). The physical mechanisms that drive the curvature of the MS at $M_* \sim 10^{10.2} M_\odot$ are still unclear.

Among the proposed mechanisms responsible for the curvature of the MS, galaxy bulge growth is most favored (Whitaker et al. 2014; Lee et al. 2015; Schreiber et al. 2015). Observationally, more massive galaxies are indeed more bulgy and tend to have higher bulge-to-total mass ratio (B/T). As shown in previous works, the central bulges of massive galaxies are generally old and dead (Pérez et al. 2013; Pan et al. 2014). Given that the bulge component contributes little to the total SFR of a galaxy, the specific star formation rate (sSFR, termed as sSFR=SFR/M_*) of a high B/T galaxy should be lower than that of a disk dominated galaxy, even they have the same M_*. This idea is supported by the work of Abramson et al. (2014), who found that when accounting for disk/bulge decomposition, the disk mass normalized SFR ($\mathrm{sSFR_{disk}}$, formulated by $\mathrm{sSFR_{disk}}$=SFR/$M_{\rm disk}$, where $M_{\rm disk}$ is the stellar mass of disk component) shows a weak dependence on M_*.

Abramson et al. (2014) argues that the star formation in galaxies is mainly contributed from galactic disk components. However, the details of how bulges affect the star formation activities in galaxies remain to be explored. To better understand the role of bulges in shaping the MS relation, in this Letter, we use the *GALEX* (Martin et al. 2005) and SDSS (York et al. 2000) data to investigate the recent star formation in the central and outer regions of a large local SFGs sample. Throughout this Letter, we assume a concordance ΛCDM cosmology with $\Omega_{\rm m} = 0.3$, $\Omega_\Lambda = 0.7$, $H_0 = 70$ km s^{-1} Mpc^{-1}, and a Kroupa (2001) IMF.

2. METHOD AND DATA USED

To assess the role of bulges in shaping the MS, a straightforward way is to derive the sSFR of the bulge component ($\mathrm{sSFR_{bulge}}$). Since the direct measure of $\mathrm{sSFR_{bulge}}$ is quite difficult, in this work we use the NUV–$r_{\rm bulge}$ color as a $\mathrm{sSFR_{bulge}}$ indicator. The NUV–r is more tightly correlated with sSFR than the $u-r$ color, especially at the low sSFR end (Salim 2014). This is not surprised because the UV luminosity $L_{\rm UV}$ is an SFR indicator (e.g., Kennicutt 1998) and NUV–r is thus a proxy of SFR/$L_{\rm r}$, where $L_{\rm r}$ is the r-band luminosity. Thus the NUV–r actually tells one the luminosity weighted sSFR.

Traditionally, a bulge+disk decomposition is required if one wants to derive the NUV–$r_{\rm bulge}$. Unfortunately, the *GALEX* imaging has a relatively low resolution (The *GALEX* NUV image has a resolution of 1 pixel=1.″5 and a point spread function (PSF) with full width at half-maximum (FWHM)=5.″3). Therefore a reliable bulge+disk decomposition procedure can

panzz@shao.ac.cn, linwp@shao.ac.cn, xkong@ustc.edu.cn
[1] Key laboratory for research in galaxies and cosmology, Shanghai Astronomical Observatory, Chinese Academy of Science, 80 Nandan Road, Shanghai, 200030, China
[2] Center of Astrophysics, University of Science and Technology of China, Jinzhai Road 96, Hefei 230026, China
[3] Key Laboratory for Research in Galaxies and Cosmology, USTC, CAS, China
[4] Purple Mountain Observatory, Chinese Academy of Sciences, 2 West-Beijing Road, Nanjing 210008, China
[5] School of Astronomy and Space Science, Sun Yat-Sen University, Guangzhou, 510275, China
[6] CSIRO Astronomy & Space Science, Australia Telescope National Facility, PO Box 76, Epping, NSW 1710, Australia
[7] Institute of Space Sciences, Shandong University, Weihai, 264209, China

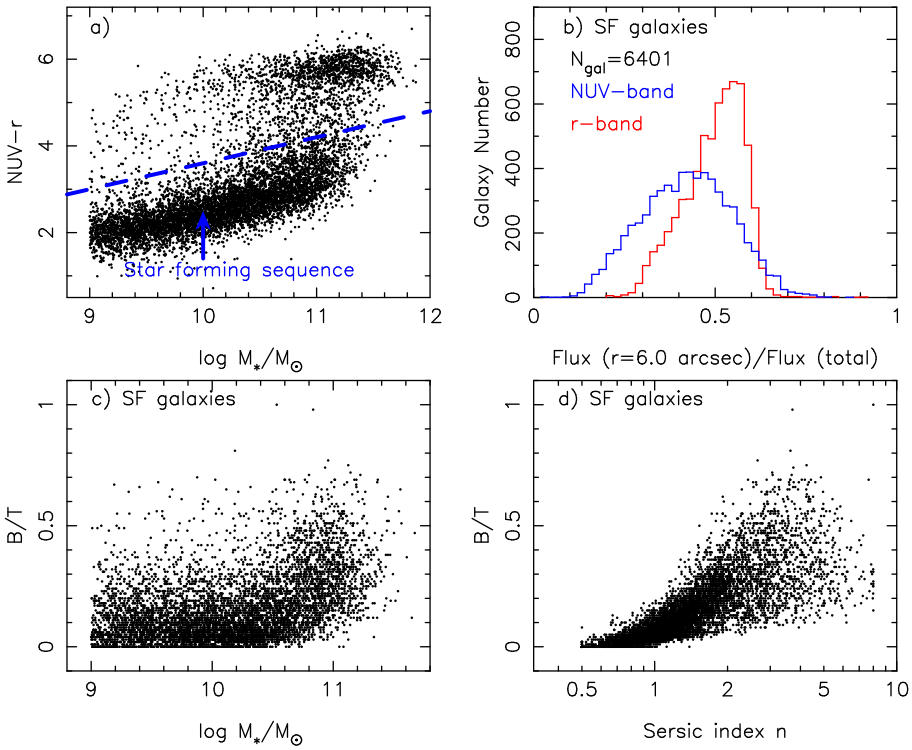

FIG. 1.— a): the color–magnitude diagram. The star forming galaxies (SFGs) are selected by the blue-dashed line. b): The $f_{\rm central}$ distribution of SFGs, where $f_{\rm central}$ was defined as $f_{\rm central} = {\rm Flux}_{r=6.''0}/{\rm Flux}_{\rm total}$. The *GALEX* NUV and SDSS *r*-band is shown in blue and red histograms, respectively. Panel c): the B/T–M_* diagram of SFGs. Panel d): the B/T–Sérsic index *n* diagram of SFGs.

be done only for galaxies with large angular sizes, which will yield a very small sample size. To investigate a large sample, in this work we instead measure the NUV–*r* color of the central region of a galaxy (NUV–$r_{\rm central}$) as the representative of NUV–$r_{\rm bulge}$ of the galaxy. We refer the central region to be $R_{\rm central} \approx R_{50}$, where R_{50} is the radius enclosing 50% of the SDSS *r*-band petrosian flux. By doing this, one can simply perform aperture photometry to obtain NUV–$r_{\rm central}$ for a galaxy sample with similar angular sizes.

Following Wang et al. (2010), we have constructed a UV-optical matched photometric catalog. This catalog contains about 220,000 galaxies with uniform photometric measurements on the resolution and PSF-matched *GALEX*+SDSS images, which are cross-matched between the SDSS DR8 (Aihara et al. 2011) spectroscopic galaxies and the *GALEX* GR6 database. For each galaxy, the fluxes were measured using 5 different apertures, with r =[1.5, 3.0, 6.0, 9.0, 12.0] $''$, in the FUV, NUV, u,g,r,i,z bands. We also measure the total magnitude of the galaxies with SExtractor (Bertin& Arnouts 1996). All the magnitudes have been corrected for galactic extinction using the galactic dust map (Schlegel, Finkbeiner & Davis 1998). The details of data reduction procedure can be found in Wang et al. (2010) and Pan et al. (2014).

To ensure that the measured central NUV–*r* color is not significantly affected by the relatively poor resolution of the *GALEX* images, we limit the sample galaxies with $R_{50} \sim 6.''0$. Our sample selection criteria are as follows:

(1) minor–major axis ratio $b/a > 0.5$, to minimize dust reddening effect;

(2) $4.''0 < R_{50} < 8.''0$, to ensure that the chosen central aperture encloses $\sim 50\%$ of the total flux of a galaxy;

(3) $z = [0.005, 0.1]$, where z is the SDSS spectroscopic redshift;

(4) $m_{\rm NUV} < m_{\rm limit}$, where $m_{\rm limit} = 23.0$ mag is the limited magnitude in the NUV band;

(5) stellar mass $M_* > 10^{9.0}\ M_\odot$.

The selected sample contains 8200 galaxies. We note that this sample is not volume-completed and our conclusions do not rely on the selection completeness in the volume. The stellar mass M_* used in this Letter was drawn from the JHU/MPA database [8]. Since all AGNs in our sample are narrow-line (obscured) AGNs, there should be no contribution from AGN continuum to the measured NUV–*r* index.

The properties of our sample galaxies are shown in Figure 1. panel a) is the color magnitude diagram. We select SFGs with NUV–r<$0.6 \times M_* - 2.4$ (the blue dashed line), where M_* is logarithm stellar mass. In total, a sample of 6401 SFGs is assembled. Panel b) shows the flux fraction distribution enclosed in the central $R = 6.''0$ aperture for the selected SFGs. One can see that the central aperture encloses $\sim 50\%$ of the *r*–band total flux. In panel c), we show the bulge-to-total ratio B/T as a function of M_*. The B/T is from the disk+bulge decomposition on the SDSS *r*-band imaging (Simard et al. 2011). As can be seen, the B/T distribution is significantly different at $M_* < 10^{10.2} M_\odot$ and $M_* > 10^{10.2} M_\odot$, in the sense that more massive galaxies have higher B/T values. However, the majority of SFGs have a B/T<0.5. Therefore, the chosen aperture of $r_{\rm central} \simeq R_{50}$ is enough to separate the bulges from the disk components for the SFGs. Panel d) presents B/T as a function of the Sérsic index *n* of the galaxy. Here *n* is fitted with a pure Sérsic model (see Simard et al. (2011) for details). As also shown in Simard et al. (2011), B/T increases with *n*. Below we present our analysis results for the sample of selected SFGs.

3. THE DEPENDENCE OF NUV–$R_{\rm CENTRAL}$ AND NUV–$R_{\rm OUTER}$ ON M_*

[8] http://www.mpa-garching.mpg.de/SDSS/DR7

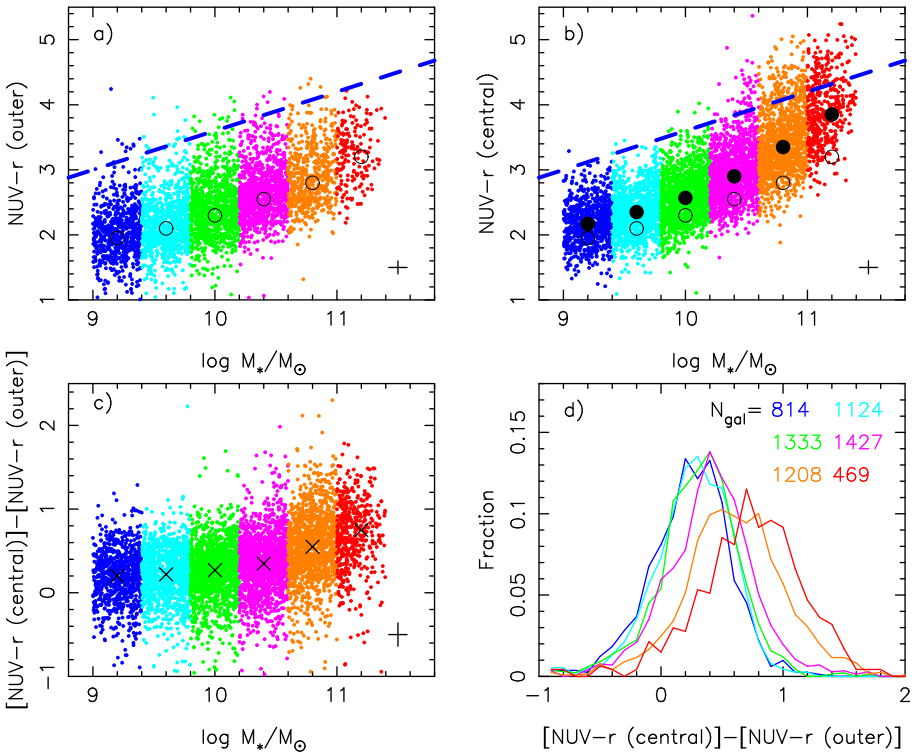

FIG. 2.— a):The relation between NUV–$r_{\rm outer}$ and M_* for SFGs, where NUV–$r_{\rm outer}$ is the color index measured outside the r =6.″0 aperture. The color represent galaxies with different M_*. The median values of NUV–$r_{\rm outer}$ values are denoted in black open circles. The blue dashed line denotes our SFGs selection criterion. b): The relation between NUV–$r_{\rm central}$ and M_*. Median values are shown in black filled circles. c): [NUV–$r_{\rm central}$]–[NUV–$r_{\rm outer}$] as a function function of M_*. Median values are shown in black crosses. d): the normalized [NUV–$r_{\rm central}$]–[NUV–$r_{\rm outer}$] distributions. The colors represent different mass bins.

Figure 2 presents the outer and central NUV–r for our sample of SFGs. Here the outer/central region of a galaxy refers to the part out/within a circular aperture of radius R = 6.″0. The SFGs are divided in 6 mass bins. As one can see from panel a), the NUV–$r_{\rm outer}$ is redder for more massive galaxies. However, no turning over is seen at $\log(M_*/M_\odot)$=10.2. In panel b), we show the [NUV–$r_{\rm central}$]–M_* diagram. For comparison, we overplot the median values of the NUV–$r_{\rm outer}$ as well. It is clear that the median value of NUV–$r_{\rm central}$ is only slightly redder than that of NUV–$r_{\rm outer}$ at $\log(M_*/M_\odot)$<10.2, while the discrepancy between the two becomes larger at higher masses. Panel c) shows the discrepancy ([NUV–$r_{\rm central}$]–[NUV–$r_{\rm outer}$]) between the two as a function of M_*. Note that we do not apply the internal extinction correction for the NUV–r measurements. If the extinction correction is similar for these two color indices, then [NUV–$r_{\rm central}$]–[NUV–$r_{\rm outer}$] reflects the intrinsic difference in color, and then the difference in sSFR. As one can see, this relation bends at $\log(M_*/M_\odot)\sim$10.2, which is similar to the MS. In panel d), we show the [NUV–$r_{\rm central}$]–[NUV–$r_{\rm outer}$] distribution. Strikingly, the three mass bins with $\log(M_*/M_\odot)$<10.2 exhibit similar distributions peaked at [NUV–$r_{\rm central}$]–[NUV–$r_{\rm outer}$]$\sim$0.25 mag. Above $\log(M_*/M_\odot)$=10.2, the distributions start to shift redward.

In short, the results presented in Figure 2 support the argument that the bend of the MS is indeed attributed to the presence of red bulges in massive galaxies. This findings also help one in better interpreting the increasing intrinsic scatters of the MS with M_* (Guo et al. 2013, 2015). Based on the large sample, this result should be reliable in a statistical sense. Interestingly, we find the trend that NUV–$r_{\rm central}$ is only 0.25 mag redder than NUV–$r_{\rm outer}$ holds for a mass range of $\log(M_*/M_\odot)$<10.2. This indicates that the central regions of less massive galaxies still have quite high $\rm sSFR_{central}$. This finding suggests that the mechanisms driving bulge growth of low-mass galaxies is similar to those regulating disk growth. In other words, bulges in low mass-SFGs tend to be psuedo type. Given this, in the next section, we will investigate the correlations of n with NUV–r as well as B/T.

4. WHAT LEADS TO DEAD BULGES?

Figure 2 supports that the red bulges of $\log(M_*/M_\odot) > 10.2$ galaxies are responsible (at least partly) for the turning over of the MS relation. In this section we address how B/T and n correlate with the read-and-dead of central bulges.

We first divide the SFGs into two categories with n<2.0 and n>2.0. In each n bin, we investigate the behavior of [NUV–$r_{\rm central}$]–[NUV–$r_{\rm outer}$] as a function of B/T. We have checked that galaxies with different n in fact have indistinguishable [NUV–$r_{\rm outer}$]–M_* relations, thus the differences of [NUV–$r_{\rm central}$]–[NUV–$r_{\rm outer}$] between different subsamples reflect their different [NUV–$r_{\rm central}$] distributions. In the upper panels of Figure 3, we show the [NUV–$r_{\rm central}$]–[NUV–$r_{\rm outer}$] distributions as a function of B/T for the SFGs with n<2.0. In each mass bin, the SFGs are split into 3 B/T bins. Each B/T bin includes a similar galaxy number. As shown in Figure 3, the [NUV–$r_{\rm central}$]–[NUV–$r_{\rm outer}$] distributions are not strongly dependent on B/T. However, at $\log(M_*/M_\odot) < 10.8$, SFGs that with the lowest B/T tend to have bluer [NUV–$r_{\rm central}$]–[NUV–$r_{\rm outer}$] than the other two B/T bins. In the lower panels of Figure 3, we show the results for those with n>2.0. Compared to the SFGs with n<2.0, the [NUV–$r_{\rm central}$]–[NUV–$r_{\rm outer}$] distributions of SFGs with n>2.0 are broader. As one can see, galaxies with n>2.0 dominate the red [NUV–$r_{\rm central}$]–[NUV–$r_{\rm outer}$] end. Similarly, the

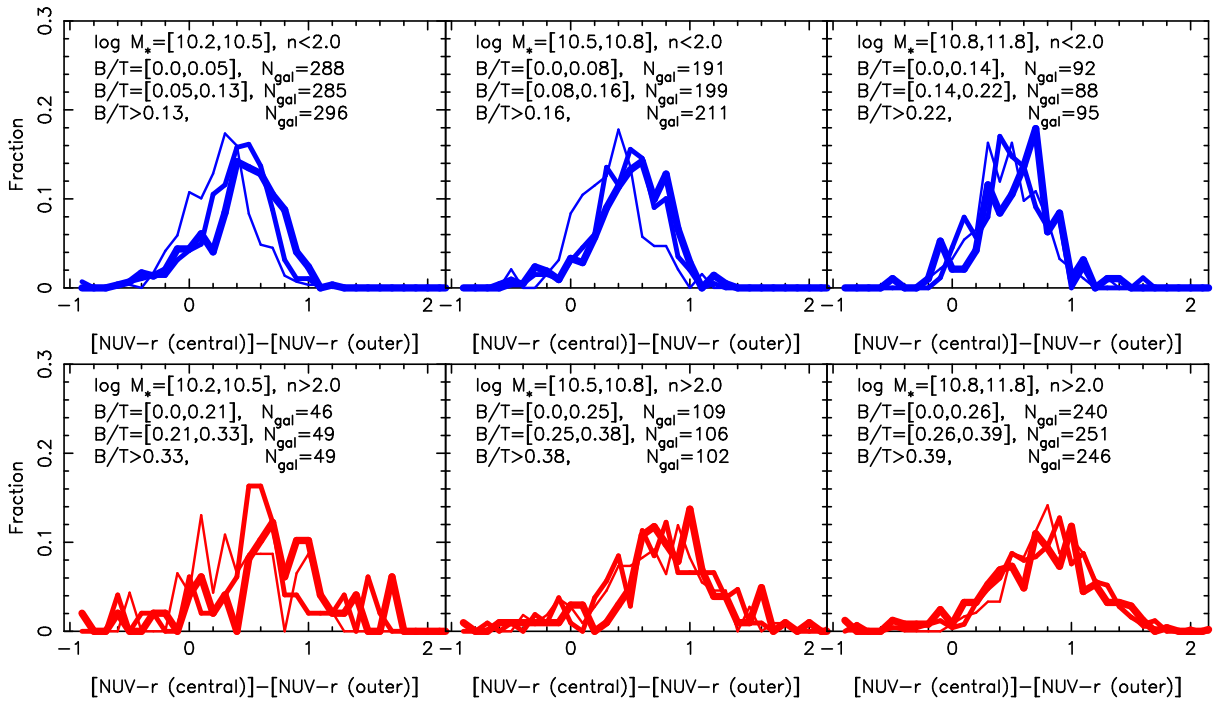

FIG. 3.— The [NUV−$r_{\rm central}$]–[NUV−$r_{\rm outer}$] distributions for the log($M_*/M_\odot$)>10.2 SFGs with n<2.0 (upper panels) and n>2.0 (upper panels) . From left to right, we show the result for different mass bins. In each mass bin, we further divide the SFGs into 3 small bins according to their B/T values. SFGs of the lowest B/T values are shown in thinnest lines, while those with highest B/T are shown in thickest lines. In each bin, the number of the SFGs are marked.

[NUV−$r_{\rm central}$]–[NUV−$r_{\rm outer}$] distributions are not strongly dependent on B/T.

In Figure 4, we investigate the dependence of [NUV−$r_{\rm central}$]–[NUV−$r_{\rm outer}$] on n. To minimize the B/T effects, we show the results in two fixed B/T bins, with B/T=[0.1,0.25] and B/T=[0.25,0.4]. In both B/T bins, Figure 4 clearly shows that the [NUV−$r_{\rm central}$]–[NUV−$r_{\rm outer}$] distributions are significantly different for the n<2.0 and n>2.0 SFGs. Note that the result of the log ($M_*/M_\odot$)=[10.2,10.5] bin may be affected by the relatively small number of n>2.0 SFGs. Moreover, one can see the n>2.0 SFGs with B/T=[0.1,0.25] can have a redder [NUV−$r_{\rm central}$]–[NUV−$r_{\rm outer}$] distribution than that of the n<2.0 SFGs with B/T=[0.25,0.4]. Thus Figure 3 Figure 4 suggest that the star formation of bulges is more strongly dependent on n than on B/T.

5. DISCUSSION

The NUV−r color is a good proxy of sSFR. However, the color index is usually affected by metallicity and dust reddening. It is thus necessary to assess the impacts of metallicity and dust extinction on our results. In Figure 2, we draw that nearly all galaxies have their NUV−$r_{\rm central}$ and NUV−$r_{\rm outer}$ bellow 5.0. Over this range, NUV−r is mainly determined by sSFR, rather than metallicity (Kaviraj et al. 2007a,b). Thus metallicity should has little influence on our results. On the other hand, if the dust reddening discrepancy between NUV−$r_{\rm central}$ and NUV−$r_{\rm outer}$ increases with M_*, then the results of Figure 2 are expected. However, Figure 3 reveals that this should not be the case because at fixed n, the peaks of the [NUV−$r_{\rm central}$]–[NUV−$r_{\rm outer}$] distributions do not shift redward with increasing M_*. Therefore the increasing color discrepancy between NUV−$r_{\rm central}$ and NUV−$r_{\rm outer}$ with M_* shown in Figure 2 can only be explained by the existence of evolved bulge stellar population in more massive SFGs.

Figure 3 and Figure 4 support that the color of bulges, or the sSFR$_{\rm bulge}$ is strongly dependent on n. Previous works found that n is very tightly correlated with quiescence. Above a critical n of $n_c \sim 2.0-2.5$, galaxies are mostly quenched (Bell et al. 2004; Drory& Fisher 2007; Bell et al. 2012; Cheung et al. 2012). A high n_g also indicates a dense galaxy bulge. Quenched galaxies mostly host dense cores, however, galaxies with dense cores do not need to be quenched (Cheung et al. 2012; Fang et al. 2013). Figure 3 and Figure 4 indicate that the reddest bulges mostly have n>2.0. However, high n SFGs do not need to have red bulges. This is consistent with the findings of Cheung et al. (2012) and Fang et al. (2013).

The dense red bulges of SFGs may imply their formation histories. As already known, there exists two types of bulges, which are the so-called "classical bulges" and "psuedobulges". The classical bulges have steep central light profile (hence dense central stellar density) and are believed to form through major mergers coupled with a central starburst event, during which the available fuel is exhaust relatively quickly. Given this, it is thus not surprised to find that part of the high n SFGs have a red NUV−$r_{\rm central}$. In contrast, psuedobulges are the bulges that have disk-like features and believed to be the products of secular evolution (see Kormendy & Kennicutt (2004) for a review). Figure 3 and Figure 4 show that galaxies with low n have bluer [NUV−$r_{\rm central}$]–[NUV−$r_{\rm outer}$] distributions, indicating more SFR in their central regions. This is consistent with the findings that psuedobulges have more gas and SFR than classical bulges (Fisher 2006; Fisher et al. 2013).

At this point it is necessary to discuss the n composition of SFGs. Figure 5 shows the fractions of SFGs with n>2.0 ($f_{\rm n>2.0}$) as a function of M_*. One can see that the $f_{\rm n>2.0}$ is quite low at $M_* < 10^{10.2} M_\odot$ but rapidly increases to 80%– 90% at $M_* \sim 10^{11.0} M_\odot$. For comparison, we overplot the $f_{\rm n>2.0}$ of the SFGs sample from Pan et al. (2015), which is volume-completed to $M_* \sim 10^{9.0} M_\odot$ at $z < 0.05$. One can see that the

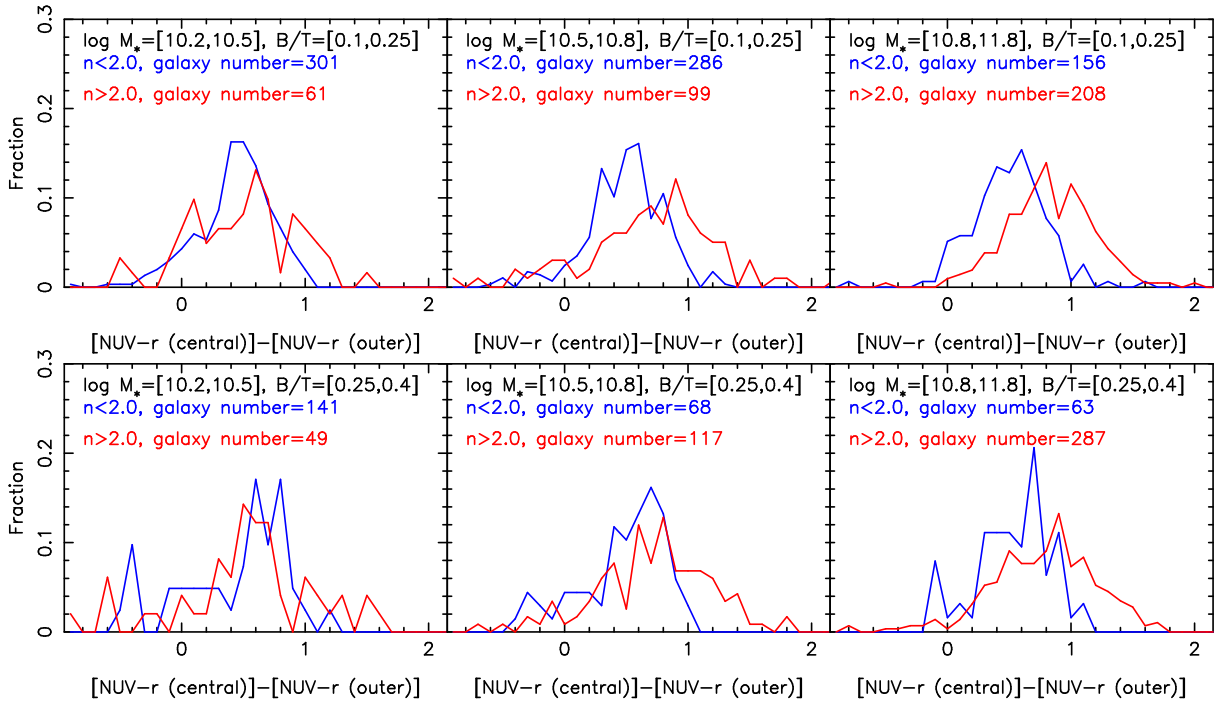

FIG. 4.— The [NUV−$r_{\rm central}$]–[NUV−$r_{\rm outer}$] distributions for the log($M_*/M_\odot$)>10.2 SFGs with B/T=[0.1,0.25](upper panels) and B/T=[0.25,0.4]. From left to right, we show the result for different mass bins. SFGs with n<2.0 are shown in blue, while those with n>2.0 are in red. In each bin, the number of the SFGs are marked.

two SFGs sample exhibit similar trends. Given this, the MS is expected to turn flatten owing to the existence of large portion of high n SFGs at the high masses.

Strikingly, [NUV−$r_{\rm central}$]–[NUV−$r_{\rm outer}$] is found to have a weak dependence on B/T at $M_* > 10^{10.2}M_\odot$, regardless of n. It is not straightforward to interpret this result. We argue that this may be due to the complex mechanisms that drive the increasing of the B/T. The increasing of B/T can either be due to secular evolution, or due to an intense central star formation episode. In the former case one sees that high B/T SFGs tend to have low $\rm SFR_{bulge}$, while in the latter the situation is reversed. Observationally, both processes can occur in a SFG sample. Even for individual galaxies, they can possibly undergo both processes during their evolution. Therefore, for a SFG that with a classical bulge (or a high n), the mixture of the two processes will drive its $\rm SFR_{bulge}$ showing a weak dependence on B/T.

For the low n SFGs whose central bulges are proposed to mainly form through secular evolution, we do observed galaxies with lowest B/T have bluest [NUV−$r_{\rm central}$] at $M_* < 10^{10.8}M_\odot$. However, this trend does not hold when comparing the results between the middle and the high B/T bins. To interpret this result, one must have a comprehensive picture of the bulge formation history of massive galaxies. In a recent work, Erwin et al. (2015) shows evidence that the inner most region of some psuedobulges are imbedded with a classical bulge, suggesting that our previous proposed bulge formation pictures are over simple. We suggest a comprehensive understanding of bulge formation is needed to fully explain the findings presented in this work.

6. CONCLUSION

In this Letter, we investigate the role of bulges in shaping the M_*–SFR relation by comparting the NUV−r color in the central $r < R_{50}$ regions to that of the outer regions for a sample of 6401 local star-forming galaxies. We find that at $M_* < 10^{10.2}M_\odot$, NUV−$r_{\rm central}$ is on average only ∼0.25 mag redder than NUV−$r_{\rm outer}$. Above $M_* = 10^{10.2}M_\odot$, [NUV−$r_{\rm central}$]–[NUV−$r_{\rm outer}$] becomes redder when increasing M_*, indicating the existence of more evolved bulges at the massive end. For the galaxies with $M_* > 10^{10.2}M_\odot$, We find that those with reddest [NUV−$r_{\rm central}$]–[NUV−$r_{\rm outer}$] are preferentially to have large Sérsic index n, even at fixed B/T and M_*. This suggests that $\rm sSFR_{bulge}$ is more strongly dependent on n (or central mass density) than on B/T. We conclude that the increasing fraction of low-sSFR dense bulges in $M_* > 10^{10.2}M_\odot$ galaxies, rather than high B/T, is responsible for the flattened slope of the M_*–SFR relation at high masses.

This work was supported by the NSFC projects (Grant Nos. 11473053, 11121062, 11233005, U1331201, U1331110, 11225315, 1320101002, 11433005, and 11421303), the National Key Basic Research Program of China (Grant No. 2015CB857001), the “Strategic Priority Research Program the Emergence of Cosmological Structures” of the Chinese Academy of Sciences (Grant No. XDB09000000), the Specialized Research Fund for the Doctoral Program of Higher Education (SRFDP, No. 20123402110037), and the Chinese National 973 Fundamental Science Programs (973 program) (2013CB834900, 2015CB857004).

REFERENCES

Abramson K., et al., 2014, ApJ, 785L, 36A
Aihara, H., Allende Prieto, C., An, D., et al. 2011, ApJS, 193, 29
Bell, E. F., McIntosh, D. H., Barden, M., et al. 2004, ApJ, 600, L11
Bell, E. F., van der Wel, A., Papovich, C., et al. 2012, ApJ, 753, 167

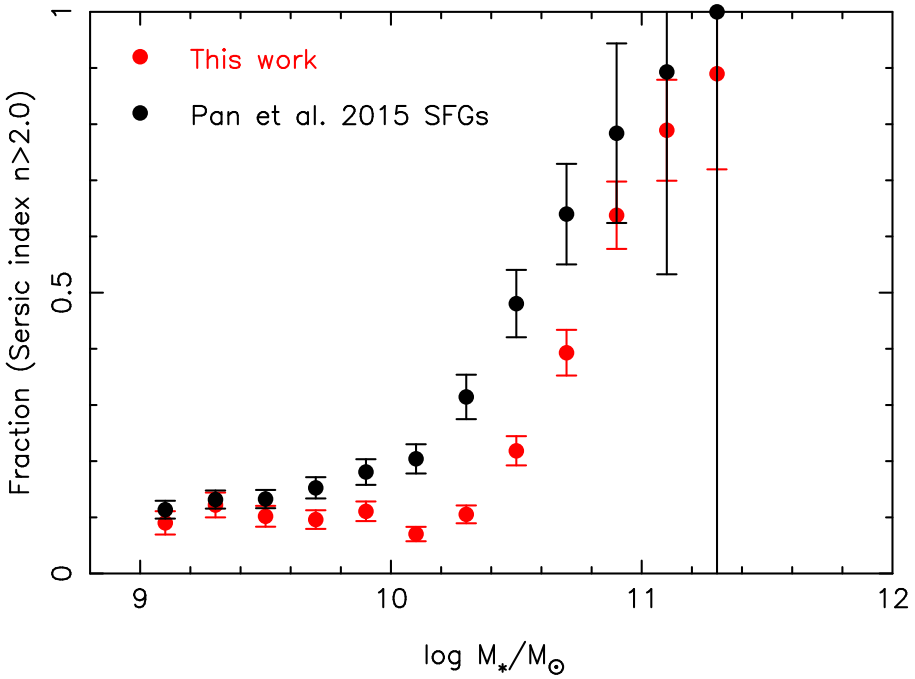

FIG. 5.— The fraction of SFGs that with n>2.0 as a function of M_*. Data points are calculated in the M_* bin size of ΔM_*=0.2 dex. The red symbols are calculated from the SFGs sample used in this work, while the black symbols are from the SFGs of Pan et al. (2015).

Bertin, E., & Arnouts, S. 1996, A&AS, 117, 393
Brinchmann, J., Charlot, S., White, S. D. M., et al. 2004, MNRAS, 351, 1151
Cheung, E, Faber, S., Koo, D., et al. 2012, ApJ, 760, 131
Daddi, E., Dickinson, M., Morrison, G., et al. 2007, ApJ, 670, 156
Drory, N., & Fisher, D. B. 2007, ApJ, 664, 640
Elbaz, D., Daddi, E., Le Borgne, D., et al. 2007, A&A, 468, 33
Erwin, P., Saglia, R. P., Fabricius, M., et al. 2015, MNRAS, 446, 4039
Fang, J. J., Faber, S. M., Koo, D. C., & Dekel, A. 2013, ApJ, 776, 63
Fisher, D. B., & Drory, N. 2008, AJ, 136, 773
Fisher, D. B. 2006, ApJ, 642, L17
Fisher, D. B., Bolatto, A., Drory, N., et al. 2013, ApJ, 764, 174
Fisher, D. B., & Drory, N. 2011, ApJ, 733, L47
Guo, K., Zheng, X. Z., & Fu, H. 2013, ApJ, 778, 23
Guo, K., Zheng, X. Z., Wang, T., & Fu, H. 2015, ApJ, 808, L49
Kaviraj, S., Rey, S.-C., Rich, R. M., Yoon, S.-J., & Yi, S. K. 2007a, MNRAS, 381, L74
Kaviraj, S., Schawinski, K., Devriendt, J. E. G., et al. 2007b, ApJS, 173, 619
Kauffmann G., White S. D. M., Heckman T. M. et al., 2003, MNRAS, 341, 54
Kennicutt, R. C., Jr. 1998, ARA&A, 36, 189
Kormendy, J., & Kennicutt, R. C., Jr. 2004, ARA&A, 42, 603
Kroupa, P. 2001, MNRAS, 322, 231
Karim, A., Schinnerer, E., Martínez-Sansigre, A., et al. 2011, ApJ, 730, 61
Lee, N., Sanders, D. B., Casey, C. M., et al. 2015, ApJ, 801, 80
Martin, D. C., Fanson, J., Schiminovich, D., et al. 2005, ApJ, 619, L1
Mendel, J. T., Simard, L., Palmer, M., Ellison, S. L., & Patton, D. R. 2014, ApJS, 210, 3
Pan, Z., Li, J., Lin, W., Wang, J., & Kong, X. 2014, ApJ, 792, L4
Pan, Z., Li, J., Lin, W., et al. 2015, ApJ, 804, L42
Peng Y. J., et al., 2010, ApJ, 721, 193
Pérez, E., Cid Fernandes, R., González Delgado, R. M., et al. 2013, ApJ, 764, L1
Salim, S. 2014, Serbian Astronomical Journal, 189, 1
Schlegel, D. J., Finkbeiner, D. P., & Davis, M., 1998, ApJ, 500, 525S
Schreiber, C., Pannella, M., Elbaz, D., et al. 2015, A&A, 575, A74
Simard, L., Mendel, J. T., Patton, D. R., Ellison, S. L., & McConnachie, A. W. 2011, ApJS, 196, 11
Strateva, I. V et al., 2001, AJ, 122, 1861
Wang J., et al., 2010, MNRAS, 401, 433
Whitaker, K. E., van Dokkum, P. G., Brammer, G., & Franx, M. 2012, ApJ, 754, L29
Whitaker, K. E., Franx, M., Leja, J., et al. 2014, ApJ, 795, 104
York D. G, et al., 2000, AJ, 120, 1579